FACULTY OF SCIENCE
UNIVERSITY OF COPENHAGEN

# Numerical Simulation of Antiferromagnetic Order in Unconventional Pauli-Limited Superconductors

Bachelor's Thesis in Physics.
Niels Bohr Institute,
University of Copenhagen

Johannes H. J. Martiny
wgd717@alumni.ku.dk

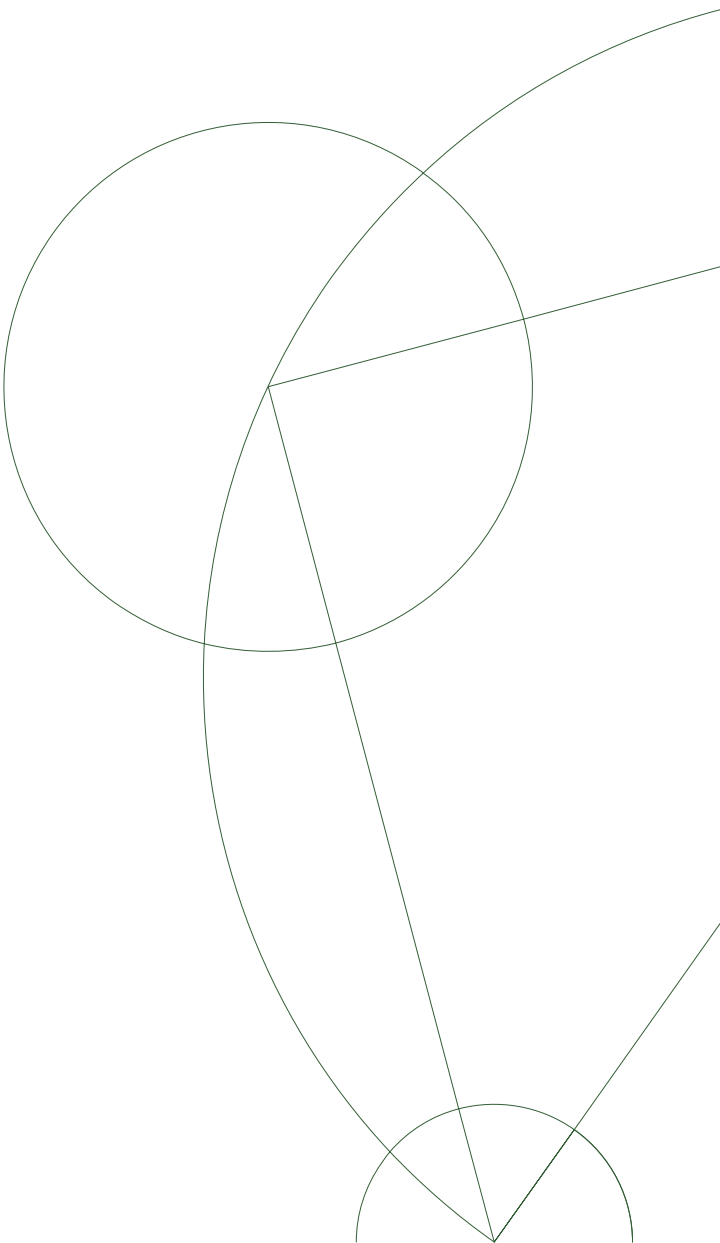

*Advisors: Brian M. Andersen*
*Maria N. Gastiasoro*

*Date: 11/06-2014*

**Abstract**

In this Bachelor's Thesis we investigate the novel phase of antiferromagnetism and superconductivity coexistence formed in the heavy fermion and strongly Pauli limited compound $CeCoIn_5$ at high fields and low temperatures. We modify the model of nesting induced antiferromagnetism in the superconducting state developed by Kato et. al. for use in a real space numerical simulation. This self-consistent simulation is developed using the formalism of second quantization and the Bogoliubov transformation. We reproduce the expected phase diagram and find the real space order in the novel phase. Finally we initialize our system outside the coexistence phase and map out the local impurity magnetization, including stabilizing a local magnetic order and detailing the correspondence with the homogeneous field-induced order.

# Contents

# 1. Introduction

Since the discovery of superconductivity by Onnes in 1911 as a sharp drop in the resistance of mercury at a critical temperature ($T_c$), microscopic theories of the phase transition have been sought. This was achieved in 1957 by Bardeen, Cooper and Schrieffer, who showed that pairs of electrons of different spin near the Fermi level become unstable toward formation of so-called Cooper pairs with the inclusion of a small attractive interaction. This attractive potential was explained as an interaction with phonons of the underlying lattice of ions.
This model adequately models many low $T_c$ superconductors yet recent discoveries of superconductors with higher critical temperatures are outside the scope of BCS theory. In such "unconventional" superconductors new pairing mechanism and the interplay of magnetism is required to understand the transition.

Superconductivity exists in regions of phase space limited by external field strength and temperature. There are two ways in which an applied magnetic field breaks the Cooper pairs. The dominant pair breaking effect in most superconductors is orbital limiting, the formation of a triangular lattice of flux cores of normal state screened by supercurrents. The superconductivity dies out completely when these flux cores start to overlap, at the upper critical field $H_{c2}$.

The less dominant effect for most superconductors is Pauli limiting, the direct pair breaking from the spin polarizing Zeeman effect. The energy of the formation of this paramagnetic state under applied field $H$ is given by $E_P = \frac{1}{2}\chi_n H^2$ where $\chi_n$ is the normal state susceptibility. As such the Pauli limiting occurs when this energy equals the condensation energy of the superconducting state $E_C = \frac{1}{2}N(0)\Delta$. Here $N(0)$ is the density of states at the Fermi level and $\Delta$ is the order parameter associated with the superconducting state in Landau theory. The Maki parameter $\alpha$ measures the ratio of these limiting fields, $\alpha = \sqrt{2}\frac{H_{c2}^{orb}}{H_{c2}^{P}}$, where $H_{c2}$ is the limiting field beyond which the normal state is realised. The Maki parameter is typically much less than unity [6, p. 2].

Pauli limiting becomes dominant in heavy fermions compounds such as $CeCoIn_5$ with a Maki parameter of $\alpha \approx 4.6$ [6, p. 9]. This material consists of alternating layers of superconducting $CeIn_3$ and less conducting $CoIn_2$, in a quasi-2D structure [6]. The rare earth atoms such as Ce are characterized by unfilled $f$ orbitals which form localized magnetic moments [1].

These moments are screened by the conduction electrons effectively forming elastic scattering centers (Kondo effect). Scattering off these local moments result in an heavily amplified effective electron mass. The screening interaction of conduction electrons mediate an antiferromagnetic tendency between the local moments of the lattice [3, p. 314].

In $CeCoIn_5$, which has effectively a lattice of Kondo effect impurities (Kondo lattice), these heavy fermions close to a magnetic instability seem to form d-wave pairing of Cooper pairs. This heavy fermion superconductivity is found to coexist with and enable the transition to an antiferromagnetic state in a high field low temperature region of phase space. A theory of the physics involved in this phase is given by Y. Kato, C.D. Batista and I. Vekhter ([4]), who suggest that the magnetic phase results from parallel pockets of the Zeeman split superconducting state Fermi surface connected by a single wavevector.

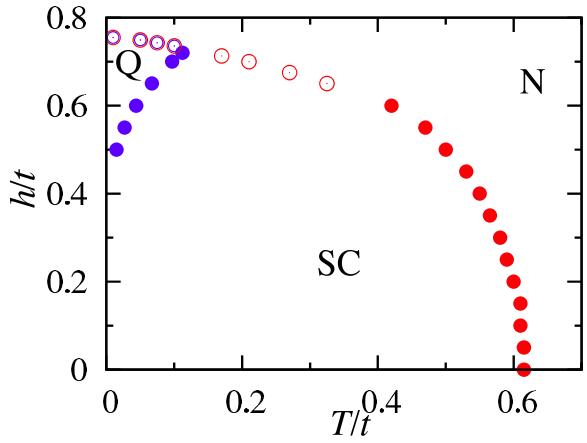


Figure 1.1.: The phase diagram obtained by Y. Kato, C.D. Batista and I. Vekhter in [4]. At high fields and low temperatures a part of the superconducting phase (SC) includes both magnetic and superconducting order (Q). Reproduction of this phase diagram will serve as a benchmark of the model developed in this thesis.

The purpose of this Bachelor's Thesis is to do a real space self-consistent numerical simulation in order to investigate the proposed magnetic state in $CeCoIn_5$, including magnetic impurity effects. To this purpose we first introduce the concepts needed to describe the interactions in a brief chapter on second quantization. The quasi-2D structure of $CeCoIn_5$ then enables us to describe the system on a 2D lattice with periodic boundary conditions in this formalism.

With the standard 2D superconductor established we attempt to replicate the system described in [4]. This includes constructing the Fermi surface, finding the nesting vectors corresponding to our system size, and then reproducing the phase diagram seen in figure 1.1. The real space model then enables us to go beyond the induced homogeneous magnetization. An inclusion of magnetic impurities will effectively introduce local magnetic fields, and a main question is then whether these local fields will expand the ordered (Q) phase of coexistence.

# 2. Second Quantization

## 2.1. Fermions

In order to write a multi-particle wavefunction for non interacting fermions in the usual QM notation we need to antisymmetrize a product of single particle wavefunctions. This is accomplished by the Slater determinant, yielding a antisymmetric superposition of states. This process is eased with the introduction of second quantization. Since individual fermions are indistinguishable we can equally well count the number of particles in each state and shift the antisymmetrization to the operators [7, p. 68]. We will be using the position basis where each state corresponds to a site on the lattice. We define the vacuum as the wavefunction with no particles in any state:

$$\Psi_{vacuum} = |000000...0\rangle \tag{2.1}$$

A state with a particle at site 2 is then simply $|010000...0\rangle$. For fermions, the Pauli principle translates to the condition that only 0 and 1 particles per state are possible per site.

We then define operators which *create* or *annihilate* different states. For fermions these are written as $c_i^\dagger, c_j$ respectively. Of these, $c_i^\dagger$ creates a particle at site $i$ and $c_j$ annihilates a particle at site j. We can in this way create any state by applying the corresponding operators to the vacuum given above.
Demanding that any combination of operators which exchange two particles changes the sign of the wavefunction we obtain the fermion anticommutation relations [7, p. 128]:

$$\{c_{i\sigma}^\dagger, c_{j\bar{\sigma}}\} = \delta_{ij}\delta_{\sigma\bar{\sigma}} \tag{2.2}$$

$$\{c_{i\sigma}, c_{j\bar{\sigma}}\} = \{c_{i\sigma}^\dagger, c_{j\bar{\sigma}}^\dagger\} = 0 \tag{2.3}$$

Where $\{a, b\}$ indicates the anticommutator of $a, b$. This ensures that the final wavefunction is antisymmetric.

The simplest operator in this formalism is the number, or density, operator $n_{i\sigma} = c_{i\sigma}^\dagger c_{i\sigma}$. Acting on a state this operator yields 0 if there is no particle at site $i$. If such a particle is present, it is annihilated and then recreated. For fermions the eigenvalues of the operator are then 0 and 1. The number operator acting on a particular site thus effectively counts the number of particles of a given spin.

## 2.2. Fourier Transform

The physics relevant to this thesis often have a simple explanation in momentum or k-space. Instead of using a position basis for the states given above we can equally well

transform to a momentum basis. This Fourier transform is defined by:

$$c_{l\sigma}^{\dagger} = \frac{1}{N} \sum_{l} e^{-i\mathbf{k}l} c_{\mathbf{k}\sigma}^{\dagger} \tag{2.4}$$

Note that we use $N$ for the length of the square lattice, which means that $N^2$ is the number of sites. As transformations involve products of operators, they are simplified using the orthogonality relation (For a proof hereof, see [5, p. 844])

$$\frac{1}{N^2} \sum_{l} e^{i(\mathbf{k}-\mathbf{k}')l} = \delta_{\mathbf{k}\mathbf{k}'} \tag{2.5}$$

This result is also of use when we investigate the onset of order in external fields. If the real space order of some quantity is of the form $G(r) = A\cos(\mathbf{Q} \cdot \mathbf{r})$, the Fourier transform is:

$$G(\mathbf{k}) = \frac{A}{2N^2} \sum_{\mathbf{l}} e^{-i\mathbf{k}\mathbf{l}} (e^{-i\mathbf{Q}\cdot\mathbf{l}} + e^{i\mathbf{Q}\cdot\mathbf{l}}) \tag{2.6}$$

$$= \frac{A}{2} (\delta(\mathbf{Q} - \mathbf{k}) + \delta(\mathbf{Q} + \mathbf{k})) \tag{2.7}$$

Demonstrating that the Fourier transform yields peaks at distinct values of $k$ corresponding to the real space ordering vector.

# 3. 2D Superconductor

## 3.1. Real Space Model

We consider a two dimensional square lattice with periodic boundary conditions. This translates to the condition that a nearest neighbour to the site closest to the right edge of the lattice is the leftmost site in the same row and so forth. The Hamiltonian describing our system will be:

$$H = -t \sum_{\langle ij \rangle \sigma} c^{\dagger}_{i\sigma} c_{j\sigma} - \mu \sum_{i\sigma} c^{\dagger}_{i\sigma} c_{i\sigma} - V \sum_{\langle ij \rangle} n_{i\uparrow} n_{j\downarrow} \tag{3.1}$$

The first term is a tight binding model of electron hopping with a constant hopping integral $t$ which will be taken as the fundamental energy unit of the problem. The summation index $\langle ij \rangle$ indicates summing over nearest neighbours only. A chemical potential is included as the second term above, acting equally on the spins. The third term represents the nearest neighbour attraction responsible for d-wave superconducting pairing of electrons of unequal spin.

A mean field transformation of the second term yields a Hamiltonian quadratic in creation and annihilation operators [2, p. 24].

$$H = -t \sum_{\langle ij \rangle \sigma} c^{\dagger}_{i\sigma} c_{j\sigma} - \mu \sum_{i\sigma} c^{\dagger}_{i\sigma} c_{i\sigma} + V \sum_{i\delta} (\Delta_{i\delta} c^{\dagger}_{i\uparrow} c^{\dagger}_{i+\delta\downarrow} + h.c.) + \text{Constant} \tag{3.2}$$

Where $\delta$ are vectors to the nearest neighbours, $\Delta_{i\delta} = \langle c_{i\uparrow} c_{i+\delta\downarrow} \rangle$ is a mean field quantity and *h.c.* indicates the hermitian conjugate. Note that constant terms will be discarded as no comparisons of the total energy are attempted in this thesis.

## 3.2. k-Space Model

In order to reproduce the Fermi surface given in [4], the simplest procedure is to transform to k-space. A Fourier transform of the form of eq. 2.4 brings the Hamiltonian to the form:

$$H = \sum_{\mathbf{k}\sigma} \epsilon_k c^{\dagger}_{\mathbf{k}\sigma} c_{\mathbf{k}\sigma} - \sum_{\mathbf{k}} (\Delta_k c^{\dagger}_{k\uparrow} c^{\dagger}_{-k\downarrow} + h.c.) \tag{3.3}$$

Where $\epsilon_k = -2t(\cos(k_x) + \cos(k_y)) - \mu$ is the band dispersion and
$\Delta_k^{d-wave} = \Delta_0(\cos(k_x) - \cos(k_y))$ is the d-wave order parameter. Defining the usual BCS s-wave order parameter as $\Delta_{\mathbf{k}}^{s-wave} = \Delta_0$, a Bogoliubov transformation (more on this later) diagonalizes the Hamiltonian and yields energies on the form $E_{\mathbf{k}} = \pm\sqrt{\epsilon_{\mathbf{k}}^2 + \Delta_{\mathbf{k}}^2}$.

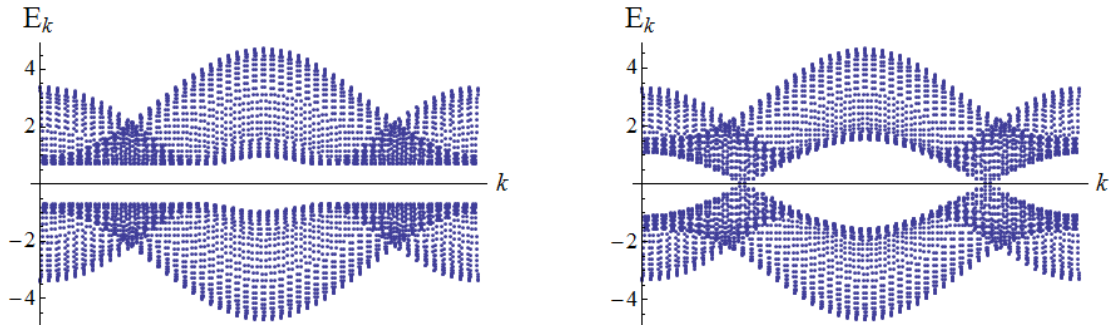


(a) s-wave (b) d-wave

Figure 3.1.: Left: Energy spectrum for the s-wave superconductor, showing a uniform gap. Right: Energy spectrum for the d-wave superconductor. The gap has nodes at the Fermi energy. These nodes will prove necessary to the formation of the coexistence (Q) phase at high fields.

The energy spectra of these different superconductivity pairing symmetries for $\Delta_0/t = 0.7$ are plotted in figure 3.1.

The d-wave pairing symmetry results in nodes in the superconductivity gap at the Fermi surface. Note that as the only lattice size effect in these spectra is the resolution, they have been computed for $N = 160$.
Since the d-wave spectrum has energies at the Fermi level, corresponding nodes appear in the Fermi surface. The symmetry and multiplicity of the four nodes are the result of $E_{\mathbf{k}}$ being symmetric in $\pm k_x$, $\pm k_y$.

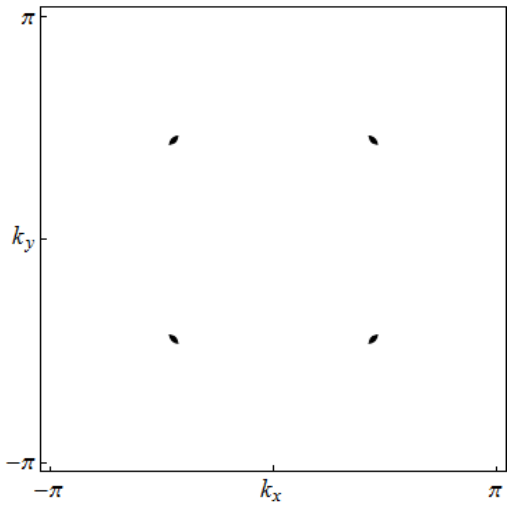


Figure 3.2.: Fermi surface for a d-wave superconductor, showing a nodal structure.

# 4. Magnetic Order

## 4.1. Fermi Surface and Nesting

With the k-space model in place, we now consider the influence of an external magnetic field. If we align the field in the spin quantization direction (chosen to be the in-plane direction ($z$)), it acts as a Zeeman splitting of the spins. This enters the Hamiltonian as a spin-dependent chemical potential. Let the Zeeman splitting be given by $h = g\mu_B H/2$ [4], then the corresponding term is:

$$H_{Zeeman} = -h \sum_{i\sigma}^{N^2} \sigma c^{\dagger}_{i\sigma} c_{i\sigma} \tag{4.1}$$

Where $\sigma = \pm 1$ for $\uparrow, \downarrow$. Adding this to the previous model, the Fermi surface for the normal and SC phase are readily obtained.

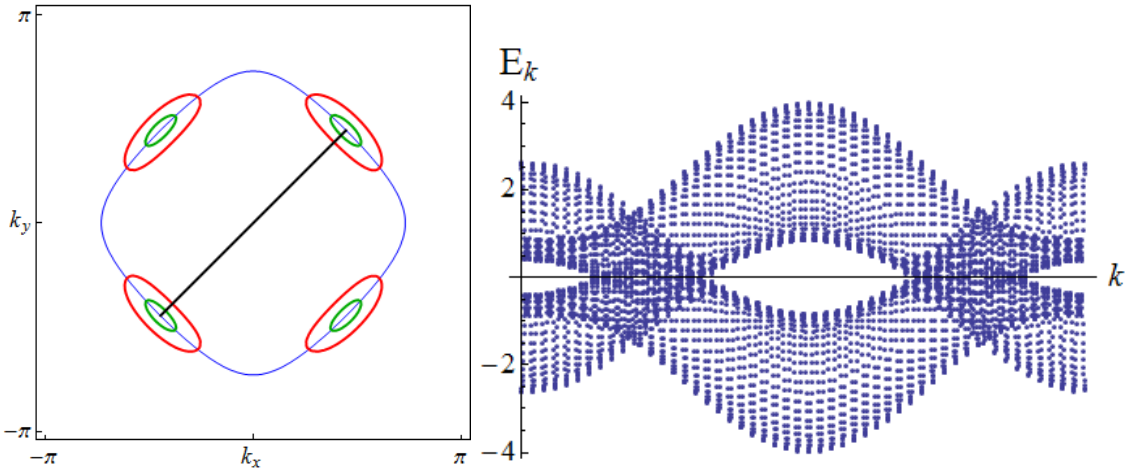


Figure 4.1.: Left: Fermi Surface for $\Delta_0/t = 0.7, \mu/t = 0.68$. The normal state surface is shown in blue and the SC state surface with field induced pockets in red ($h/t = 0.7$) and green ($h/t = 0.3$). The black line is the nesting vector $\mathbf{Q} = 0.8888(\pi, \pi)$. Right: Energy spectrum for a d-wave superconductor under applied field $h = 0.7$. The nodes are extended by the Zeeman splitting.

As examined previously in figure 3.2, the d-wave superconductivity collapses the normal state Fermi surface into a nodal structure. Figure 4.1 shows the expansion of these nodes into pockets under applied field.

To see which particles occupy these pockets we follow the method of Kato et. al. and

apply a Bogoliubov transformation. We write the usual electron creation and annihilation as a linear combination of new operators, $\gamma_{\mathbf{k}\uparrow} = u_{\mathbf{k}} c_{\mathbf{k}\uparrow} - v^*_{\mathbf{k}} c^\dagger_{-\mathbf{k}\downarrow}$, $\gamma_{\mathbf{k}\downarrow} = u_{\mathbf{k}} c_{\mathbf{k}\downarrow} + v^*_{\mathbf{k}} c^\dagger_{-\mathbf{k}\uparrow}$ where $\gamma$ are Bogoliubov quasiparticle operators. If we require that this transformation be unitary, the quasiparticle operators are found to obey fermion anticommutation relations. Writing $E_k = \sqrt{\epsilon_k^2 + \Delta_k^2}$, this transformation diagonalizes the Hamiltonian [4]:

$$H = \sum_{\mathbf{k}} (E_k - h)\gamma^\dagger_{\mathbf{k}\uparrow}\gamma_{\mathbf{k}\uparrow} + (E_k + h)\gamma^\dagger_{-\mathbf{k}\downarrow}\gamma_{-\mathbf{k}\downarrow} \tag{4.2}$$

We see that the Zeeman splitting favours the creation of spin up Bogoliubov quasiparticle pockets. These pockets form pairwise parallel regions on the Fermi surface connected by the same wave vector. We call these regions nested, with nesting vector $\mathbf{Q}$ (plotted in figure 4.1 in black). We expect any order between these pockets to be modulated with the nesting vector.

Note that the chemical potential has been changed from the value of $\mu/t = 0.749$ used in ([4]) to obtain a periodic magnetic order on the lattice. Since we will soon introduce an antiferromagnetic order modulated by $\cos(\mathbf{Q} \cdot \mathbf{r})$, the periodic boundary conditions imply that the lattice size must fulfill $(Q_x \cdot N) = 2\pi n$ to be periodic in (x). The same argument holds for $Q_y$. To this effect system sizes of $N = l \cdot 9, l \in \mathbb{N}$ are chosen which fulfill this criterion for a nesting vector of $\mathbf{Q} = (0.8888\pi, 0.8888\pi)$, corresponding to a chemical potential $\mu/t = 0.68$. This chemical potential is found from visual inspection of the Fermi surface, varying $\mu$ to obtain the given $\mathbf{Q}$. By comparison with the Fermi surface plotted in [4], no dominant effect on the pocket size by the shifted chemical potential is observed.

## 4.2. AFM Order

The quasiparticle pockets are found by Kato et. al. to be unstable towards an antiferromagnetic ordering orthogonal to the applied field. This is modelled with a mean field term, assuming a simple spiral order modulated with the nesting vector, $m(r) = m_{\mathbf{Q}}(\cos(\mathbf{Q} \cdot r), \sin(\mathbf{Q} \cdot r), 0)$. We define the magnetization (in units of $\mu_B$) as $\mathbf{m} = g\langle \mathbf{S} \rangle$,

with Lande g factor $g \approx 2$, and include the following mean field term in the Hamiltonian:

$$H_{AFM} = -J \sum_i \mathbf{m}_i \mathbf{S}_i \tag{4.3}$$

$$= -\frac{J}{2} \sum_{i\sigma\bar{\sigma}} \mathbf{m}_i^x (c_{i^*\sigma}^\dagger \sigma_{\sigma\bar{\sigma}}^x c_{i^*\bar{\sigma}}) + \mathbf{m}_i^y (c_{i^*\sigma}^\dagger \sigma_{\sigma\bar{\sigma}}^y c_{i^*\bar{\sigma}}) \tag{4.4}$$

$$= -\frac{J}{2} \sum_i \langle c_{i\uparrow}^\dagger c_{i\downarrow} + c_{i\downarrow}^\dagger c_{i\uparrow} \rangle (c_{i\uparrow}^\dagger c_{i\downarrow} + c_{i\downarrow}^\dagger c_{i\uparrow}) \tag{4.5}$$

$$+ \frac{1}{i} (\langle c_{i\uparrow}^\dagger c_{i\downarrow} - c_{i\downarrow}^\dagger c_{i\uparrow} \rangle) \frac{1}{i} (c_{i\uparrow}^\dagger c_{i\downarrow} - c_{i\downarrow}^\dagger c_{i\uparrow}) \tag{4.6}$$

$$= -J \sum_i \langle c_{i\uparrow}^\dagger c_{i\downarrow} \rangle c_{i\downarrow}^\dagger c_{i\uparrow} + \langle c_{i\downarrow}^\dagger c_{i\uparrow} \rangle c_{i\uparrow}^\dagger c_{i\downarrow} \tag{4.7}$$

The spiral order initial conditions are then:

$$g\langle S_i^x \rangle = m_x \Leftrightarrow \tag{4.8}$$

$$(\langle c_{i\uparrow}^\dagger c_{i\downarrow} \rangle + \langle c_{i\downarrow}^\dagger c_{i\uparrow} \rangle) = m_{\mathbf{Q}} \cos(Q \cdot r_i) \tag{4.9}$$

$$g\langle S_i^y \rangle = m_y \Leftrightarrow \tag{4.10}$$

$$\frac{1}{i} (\langle c_{i\uparrow}^\dagger c_{i\downarrow} \rangle - \langle c_{i\downarrow}^\dagger c_{i\uparrow} \rangle) = m_{\mathbf{Q}} \sin(Q \cdot r_i) \tag{4.11}$$

$$\Rightarrow \tag{4.12}$$

$$\langle c_{i\uparrow}^\dagger c_{i\downarrow} \rangle = \frac{m_{\mathbf{Q}}}{2} e^{iQ \cdot r_i} \tag{4.13}$$

$$\langle c_{i\downarrow}^\dagger c_{i\uparrow} \rangle = \frac{m_{\mathbf{Q}}}{2} e^{-iQ \cdot r_i} \tag{4.14}$$

The combined Hamiltonian listed below and the initial conditions for all mean fields finishes our description of the model.

$$H = -t \sum_{\langle ij \rangle \sigma} c_{i\sigma}^\dagger c_{j\sigma} + V \sum_{i\delta} (\Delta_{i\delta} c_{i\uparrow}^\dagger c_{i+\delta\downarrow}^\dagger + h.c.) - \mu \sum_{i\sigma} c_{i\sigma}^\dagger c_{i\sigma} \tag{4.15}$$

$$- J \sum_i \left( \langle c_{i\uparrow}^\dagger c_{i\downarrow} \rangle c_{i\downarrow}^\dagger c_{i\uparrow} + \langle c_{i\downarrow}^\dagger c_{i\uparrow} \rangle c_{i\uparrow}^\dagger c_{i\downarrow} \right) \tag{4.16}$$

# 5. Numerical Simulation

## 5.1. Bogoliubov Transformation

The quadratic Hamiltonian can be rewritten in matrix form.

$$H = \frac{1}{2}(c^\dagger_{1\uparrow}...c_{1\downarrow}...c^\dagger_{1\downarrow}...c_{1\uparrow}) \begin{pmatrix} \xi_\uparrow & \Delta^* & M & 0 \\ \Delta & -\xi_\downarrow & 0 & -M \\ M^* & 0 & \xi_\downarrow & -\Delta^* \\ 0 & -M^* & -\Delta & -\xi_\uparrow \end{pmatrix} \begin{pmatrix} c_{1\uparrow} \\ c^\dagger_{1\downarrow} \\ c_{1\downarrow} \\ c^\dagger_{1\uparrow} \end{pmatrix} \tag{5.1}$$

Where $\xi_\sigma$ describe regions of nearest neighbour interaction $t$, $\Delta$ is the d-wave superconductivity and $M = \langle c^\dagger_\uparrow c_\downarrow \rangle$ is the on-site (diagonal) magnetic interaction. Note that signs are the result of interchanging the operators, e.g. the term $Ac_{i\sigma}c^\dagger_{i\sigma}$ is equivalent to $-Ac^\dagger_{i\sigma}c_{i\sigma}$ according to the anticommutation relations 2.3.

Writing the operator vectors as $\mathbf{c}, \mathbf{c}^\dagger$ and denoting the matrix by $\Xi$, we introduce a unitary transformation $U$ and define new operators $\gamma, \gamma^\dagger$:

$$\begin{aligned} \mathcal{H} &= \mathbf{c}^\dagger \Xi \mathbf{c} && (5.2) \\ &= \mathbf{c}^\dagger U U^\dagger \Xi U U^\dagger \mathbf{c} && (5.3) \\ &= \gamma^\dagger U^\dagger \Xi U \gamma && (5.4) \end{aligned}$$

Where $\gamma = U^\dagger \mathbf{c}$.
This is a Bogoliubov transformation of the old creation and annihilation operators to a linear combination of quasiparticle operators $\gamma$ as done previously for the k-space model. Written out more clearly the transformation assumes the form:

$$\begin{pmatrix} c_{i\uparrow} \\ c^\dagger_{i\downarrow} \\ c_{i\downarrow} \\ c^\dagger_{i\uparrow} \end{pmatrix} = \begin{pmatrix} \alpha^1_{in} & \alpha^2_{in} & \alpha^3_{in} & \alpha^4_{in} \\ \beta^1_{in} & \beta^2_{in} & \beta^3_{in} & \beta^4_{in} \\ \omega^1_{in} & \omega^2_{in} & \omega^3_{in} & \omega^4_{in} \\ u^1_{in} & u^2_{in} & u^3_{in} & u^4_{in} \end{pmatrix} \begin{pmatrix} \gamma_{n\uparrow} \\ \gamma^\dagger_{n\downarrow} \\ \gamma_{n\downarrow} \\ \gamma^\dagger_{n\uparrow} \end{pmatrix} \tag{5.5}$$

Note that $i, n$ range from 1 to $N^2$. The requirement that this transformation be unitary translates to the condition that the new operators be fermionic, i.e. obey the anticommutation relations given in equation 2.3.

We now demand that this transformation diagonalizes the Hamiltonian and thus obtain an expression for the transformation matrix $U$. We denote by $I$ the diagonal matrix

of energy eigenstates.

$$H = \gamma^\dagger U^\dagger \Xi U \gamma = \gamma^\dagger I \gamma \Rightarrow \tag{5.6}$$

$$U^\dagger \Xi U = I \Rightarrow \tag{5.7}$$

$$\Xi U = UI \tag{5.8}$$

This defines an eigenvalue equation for $U$, and the columns of this matrix are thus the eigenvectors of $\Xi$.

Since the Bogoliubov quasiparticle operators are fermionic, they obey Fermi-Dirac statistics. This translates to the condition $\langle \gamma_n^\dagger \gamma_n \rangle = f(E_n)$, where $f(E_n) = \frac{1}{\exp(E_n/kT)+1}$. The mean field quantities are then (see Appendix A):

$$n_{i\uparrow} = \sum_{n=1}^{4N^2} |\alpha_{in}|^2 f(E_n), \quad n_{i\downarrow} = \sum_{n=1}^{4N^2} |\omega_{in}|^2 f(E_n) \tag{5.9}$$

$$\Delta_{i\delta} = \sum_{n=1}^{N^2} \alpha_i \beta_{i+\delta}^* f(-E_n), \quad \langle c_{i\uparrow}^\dagger c_{i\downarrow} \rangle = \sum_{i=1}^{4N^2} u_{in} \beta_{in}^* f(-E_n) \tag{5.10}$$

These form the self-consistent equations needed for the numerical simulation. We now choose parameters matching the system described in [4]. To model a heavy fermion compound we find the critical J ($J_c$) for which the system becomes an antiferromagnet and choose $J < J_c$ to model a system at the edge of magnetism. In accordance with [4] we choose $J/t = 3.5$ (as $J_c \approx 3.6$ in our system ), $V/t = 3$ and choose as our initial guess for the magnetization $m(r_i) = m_{\mathbf{Q}}(\cos \mathbf{Q} \cdot r_i, \sin \mathbf{Q} \cdot r_i, 0)$ as described above.

## 5.2. Homogeneous System

Upon initializing the mean field quantities the Hamiltonian is diagonalized and the mean fields updated (Mathematica script included in Appendix B). This process is then repeated until the mean fields have stabilized or decayed. We then explore the phase diagram obtained through the alternate method of energy minimization in [4]. The result is plotted below, done in steps of $\sim 0.1$ in both $h$ and $T$.

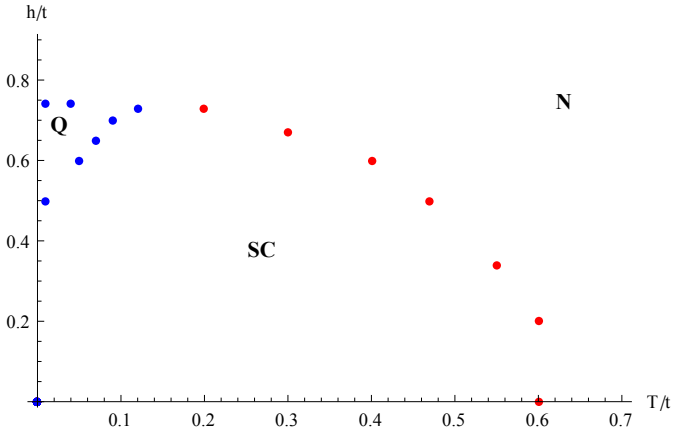


Figure 5.1.: Phase diagram showing a coexistence of superconductivity (SC) and the described magnetic order in the Q phase. Red dots indicate the superconducting phase, blue dots surround the phase of coexistence. Note that this has been computed for $N = 9$ due to time constraints of the computations. Upon increase to $N = 18$ the phase diagram appears stable.

The ordered phase is seen to decay outside a small high field low temperature region, as expected from [4]. With the phase diagram consistent, the real space order can be studied.

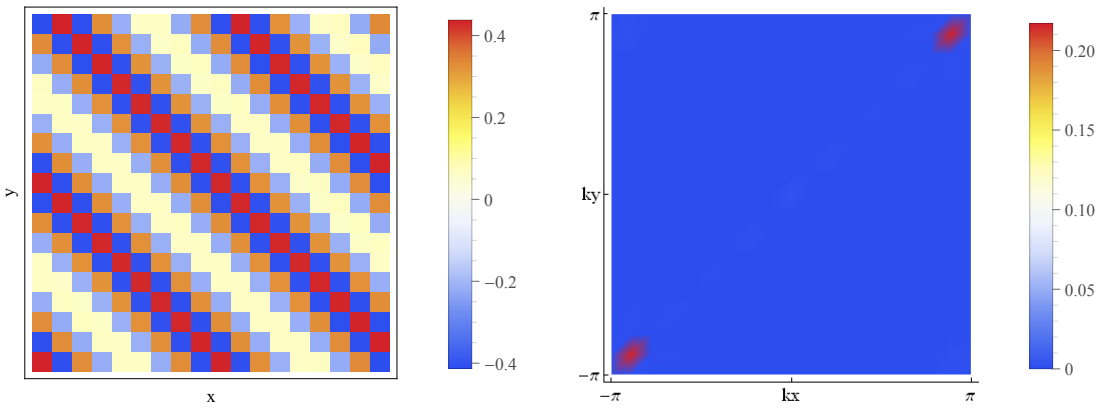


(a) Real Space (c) k Space

Figure 5.2.: Left: Arrayplot showing $m_x$ for the homogeneous stable system. Right: Fourier transform in the first Brillioun zone. The stable order is seen upon transformation to have an ordering vector corresponding to the suggested $0.8888(\pi, \pi)$.

Plotting all components of the magnetization, the $m_y$ component is seen to decay for all parameters. According to [4] this is consistent with the easy spin alignment axis in $CeCoIn_5$ being orthogonal to the plane (the (x) axis in our model).The initial spiral order thus contorts to align with the easy axis. As this is the case for all parameters the

initial guess for the magnetization is rewritten as $m(r) = m_{\mathbf{Q}}(\cos \mathbf{Q} \cdot r, 0, 0)$, to speed up computation. The $\mathbf{Q}$-order in $m_x$ is plotted in figure 5.2 for $kT/t = 0.01$ and $h/t = 0.7$.

The real space ordering is seen to stabilize as the suggested single nesting vector structure. This is evident in the Fourier transform plot in figure 5.2c, where the expected peaks at $\mathbf{k} = \mathbf{Q}, -\mathbf{Q}$ are present.

To investigate the competing orders the stabilized real space superconducting order parameter is relevant. We define the singlet and triplet superconducting order parameters as:

$$\Delta_{ij}^{(s)} = \frac{1}{2}(\langle c_{i\uparrow} c_{j\downarrow} \rangle - \langle c_{i\downarrow} c_{j\uparrow} \rangle) = \frac{1}{2}(\Delta_{ij} + \Delta_{ji}) \tag{5.11}$$

$$\Delta_{ij}^{(T)} = \frac{1}{2}(\langle c_{i\uparrow} c_{j\downarrow} \rangle + \langle c_{i\downarrow} c_{j\uparrow} \rangle) = \frac{1}{2}(\Delta_{ij} - \Delta_{ji}) \tag{5.12}$$

Where $j$ span the four nearest neighbour sites. We define the $d_{x^2-y^2}$ order parameter as:

$$\Delta^{(s,T)} = \frac{1}{4}(\Delta_{i(1,0)}^{s,T} + \Delta_{i(-1,0)}^{s,T} - \Delta_{i(0,-1)}^{s,T} - \Delta_{i(0,1)}^{s,T}) \tag{5.13}$$

Of these, the triplet order parameter is found to be approximately zero corresponding to the expected singlet superconductivity in $CeCoIn_5$ [4].
The singlet order parameter is plotted in figure 5.3 for the homogeneous system:

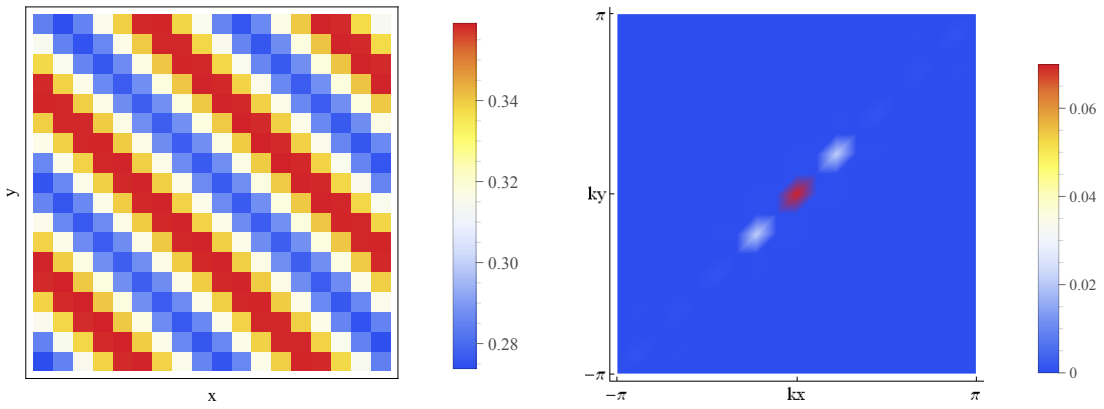


(a) Real Space (c) k Space

Figure 5.3.: Left: Arrayplot showing $\Delta_i^s$ for the homogeneous system. The order is maximally suppressed in regions of maximum amplitude of $m_x$, showing the competing orders. Right: Fourier transform in the first Brillioun zone of the reduced order parameter $\Delta_i^s - \min(\Delta_i^s)$. Note that the ordering vector of the small modulation is $2Q$, moved into the first Brillioun zone by a reciprocal lattice vector.

Note that the Fourier transform given in 5.3c is for the reduced order parameter $\Delta^s - \min(\Delta^s)$ to enhance the ordering peaks compared to the $\mathbf{Q} = 0$ peak.

The total electron density has the same modulation (see figure 5.4), a suppression in the region of highest amplitude of magnetization. As plotted in figure 5.3c this ordering is modulated with a different ordering vector than $\mathbf{Q}$. Instead, the ordering is approximately at $\pm(0.8888-1, 0.8888-1)\pi$ corresponding to an ordering vector $2\mathbf{Q}$ moved into the first Brillioun zone by a reciprocal lattice vector $2\pi(1,1)$. Such an ordering is to be expected: The density and superconductivity can not depend on the direction chosen for the magnetization, and the lowest order term coupling the density or superconductivity order parameter in a Landau expansion of the free energy is then $(n, \Delta)m^2 \sim \cos(\mathbf{Q}\cdot r)^2$ which in the Fourier transform yields peaks at $\pm 2\mathbf{Q}$.

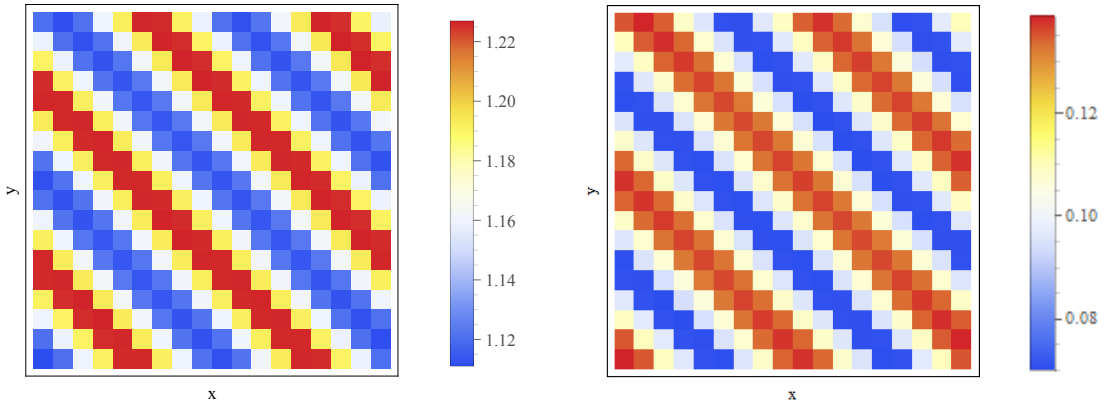


(a) $n_i$ (c) $m_z$

Figure 5.4.: Left: Arrayplot showing $\langle n_\uparrow + n_\downarrow \rangle$ for the homogeneous system. Right: $m_z$ for the homogeneous system showing the inverse modulation of the density.

Contrary to the prediction in [4] we find a magnetization component $m_z = n_\uparrow - n_\downarrow$ modulated like the total density (see figure 5.4). The relative strength of this component and the effect on the $m_x$ order is best visualized as a vector plot of the magnetization on each site, shown below (A larger plot is available in appendix C.

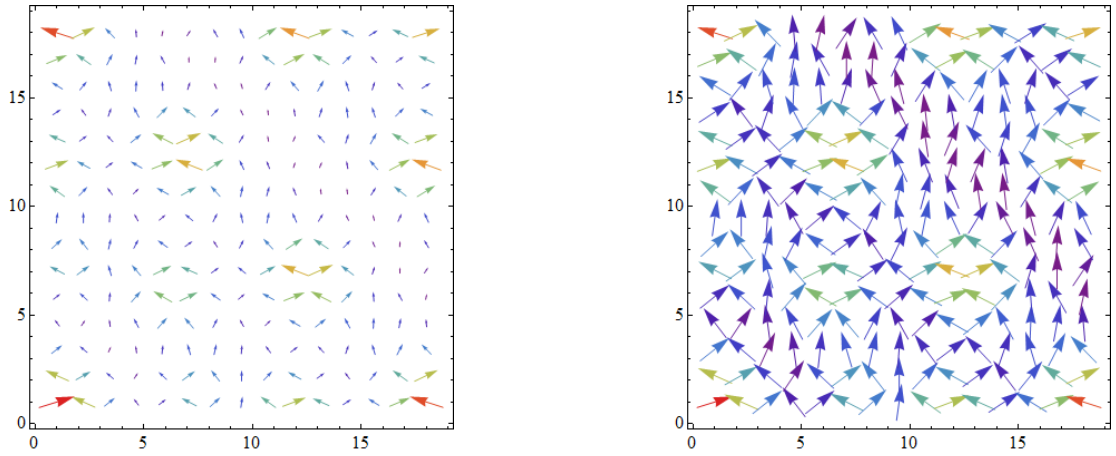


(a) Scaled in magnitude (b) Unscaled

Figure 5.5.: Left: Vector plot of the two-dimensional magnetization. Right: The same plot with constant magnitude showing the direction of vectors more clearly. The $m_x$ component is horizontal, with the $m_z$ component vertical.

## 5.3. Impurity Magnetization

With the homogeneously ordered system stabilized we can begin the study of magnetic impurities. The Hamiltonian for a local impurity magnetization is found by modelling the impurity as a fixed spin on a given site. We can then place an impurity aligned with the field of the form $\mathbf{S}_{i^*} = (0, 0, S^z_{i\sigma})$, and choose $S^z_{i^*\uparrow} = 1$:

$$H_{z-Imp} = -J_z \sum_{\sigma\sigma} \mathbf{S}_{i^*} \cdot (c^\dagger_{i^*\sigma} \sigma^x_{\sigma\bar{\sigma}} c_{i^*\bar{\sigma}}) \tag{5.14}$$

$$= -J_z \sum_{\sigma} \sigma c^\dagger_{i^*\sigma} c_{i^*\sigma} \tag{5.15}$$

Where $\sigma = \pm 1$ for $\uparrow, \downarrow$.
Equally relevant is the study of impurities in the direction of the desired magnetization component $m_x$. The same argument for $\mathbf{S}_{i^*} = (S^x_{i\sigma}, 0, 0)$ yields a different term:

$$H_{x-imp} = -J_x (c^\dagger_{i^*\uparrow} c_{i^*\downarrow} + h.c.) \tag{5.16}$$

An example of the local order for one impurity potential is given in figure 5.6 and 5.7. The ordering is not only present at the expected $\pm\mathbf{Q}$ peaks but also at the other corners of the zone. This corresponds to nesting order from both pair of pockets of the Fermi surface. This is to be expected for impurities as the local order has no predisposition to any one ordering vector by the surrounding initialized order.

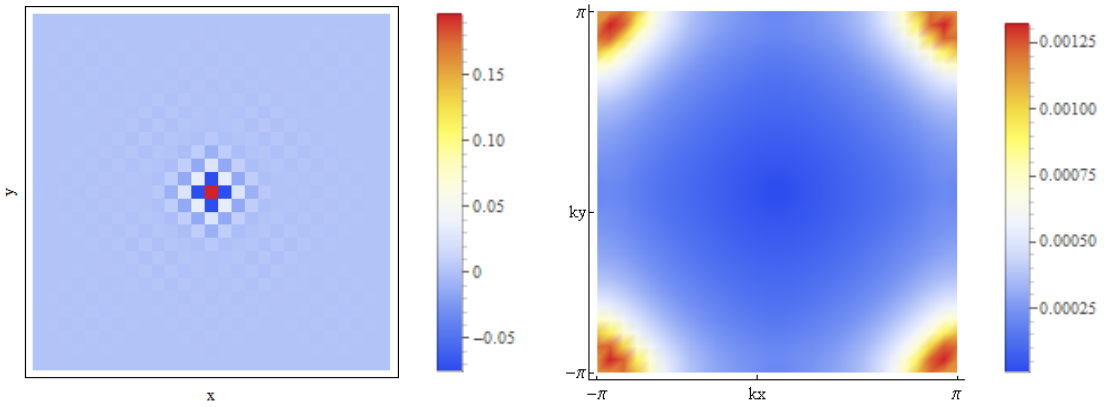


(a) Real Space (c) k Space

Figure 5.6.: Left: Arrayplot showing $m_x$ for the (x) impurity with $J_x = 0.6$ and $h = 0$.. Right: Fourier transform in the first Brillioun zone. The order has peaks from all possible nesting vectors.

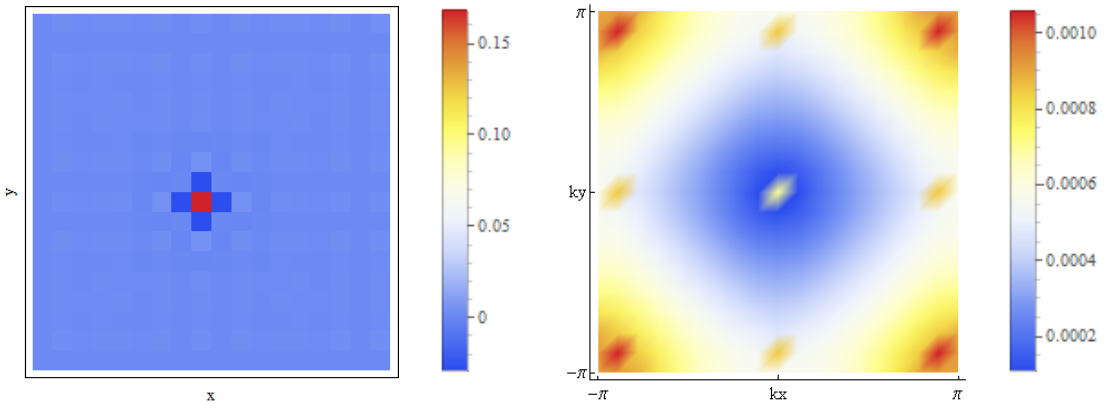


(a) Real Space (c) k Space

Figure 5.7.: Left: Arrayplot showing $m_z$ for the (z) impurity with $J_z = 0.6$ and $h = 0$. Right: Fourier transform in the first Brillioun zone. The direct magnetization is a very local response, yielding a combination of orders including at $\mathbf{Q}$.

Inducing the homogeneous $\mathbf{Q}$-order by impurity doping will require mapping out strength of the local ordering of these different impurity types. The ordering is not optimally described by the real space amplitude of magnetization but rather by the strength of the dominant order. A very strong order only at the impurity site is of little interest as this can't possibly add up to the homogeneous order with the inclusion of periodic impurities. The strength is thus best described by the amplitude of the Fourier transform at the nesting vector $\mathbf{Q}$, which will correspond to the relative strength of the desired ordering for a given impurity potential. This is plotted for both types of impurities in figure 5.8. Note that we plot only linear magnetization, as (z) impurities induce

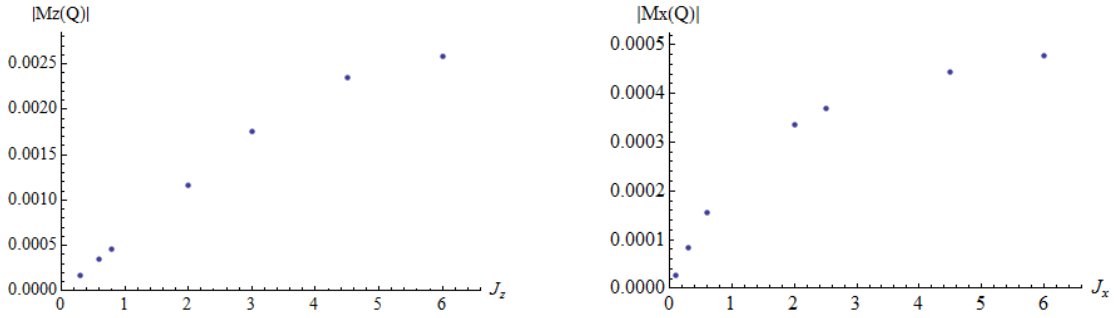


(a) (b)

Figure 5.8.: Left: $m_z(\mathbf{Q})$ for an magnetic impurity with spin along $(z)$, for a system size of $N = 18$ at $h = 0$. Right: $m_x(\mathbf{Q})$ for an magnetic impurity with spin along $x$ for a system size of $N = 27$ also at $h = 0$. The response is the expected linear mean field response decaying to an upper limiting ordered magnetization.

only finite $m_z$ and (x) impurities induce only finite $m_x$ at $h = 0$.
In the homogeneous system, the high field induced a transverse magnetization. To see whether it is possible to accomplish the same by using an impurity along the field, we choose $h/t = 0.4$ outside the high field phase but include a strong (z) impurity $J_z/t = 3$. For simplicity we choose $kT/t = 0.01$ in order to avoid thermal effects. In addition to the expected direct $m_z$ component expected from the $h = 0$ case, this stabilizes the desired finite $m_x$ component (see figure 5.9).

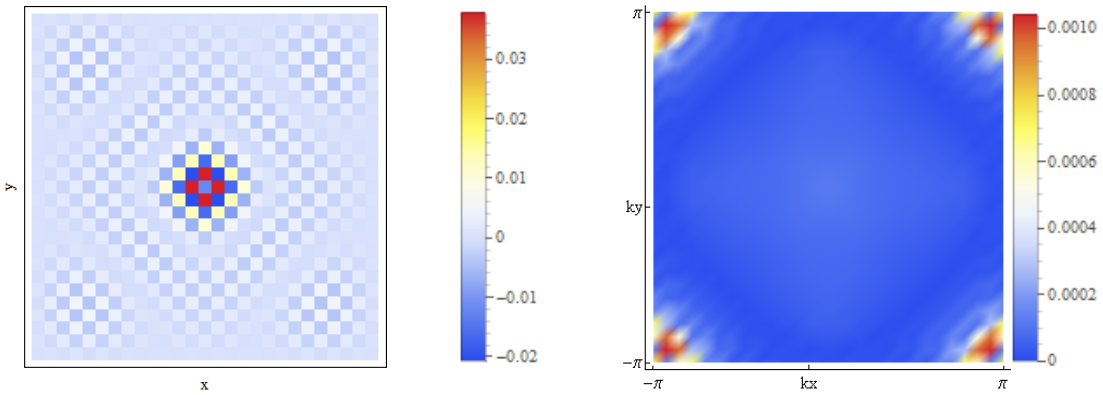


(a) Real Space (c) k Space

Figure 5.9.: Left: Arrayplot showing $m_x$ for the in-field stabilized strong, $J_z/t = 3$, (z) impurity. Right: Fourier transform in the first Brillioun zone.

# 6. Discussion

Numerically simulating our model in real space has allowed the study of stabilization of competing orders and the introduction of impurities. This is accomplished using the quasi-2D structure of $CeCoIn_5$ which we model on a discrete lattice by including periodic boundary conditions. This should in theory allow us to use an arbitrarily small system size as long as it is not shorter than the period of any of the included orders. Yet a larger system of $N = 18$ or $N = 37$ is not only advisable for precision purposes but strictly necessary when we include strong impurities.
Initializing too strong an impurity for a small system size enables the induced local order to extend over the right edge of the finite lattice through the periodic boundary conditions and interacting with the impurity from the left. In the study of single impurities and the local order thereof this invalidates the model, hence the need to choose larger system sizes for some impurities. This is the reason system sizes for impurities are alternating between $N = 18$ and $N = 27$.

Contrary to the prediction in [4] we find a non-zero $m_z$ as well as the expected $m_x$ component. As the ordering of this component mirrors the density, superconductivity and total density it is thought to be connected to the self-consistent method employed in this thesis. No effect of this non-zero component is found on region in which the expected Q-phase stabilizes, which suggest that this magnetization component has no dominant effect on the induced magnetization in $m_x$ relevant for the further impurity study. Figure 5.5 shows how the expected antiferromagnetic order is realised side by side with the finite $m_z$ component.

The homogeneous AFM studied here has been for a single nesting vector connecting pockets. As detailed in [4] a more general order is one in which we consider the nesting of both the lower left and upper right (our model), and the lower right and upper left pockets. This corresponds to a magnetization of the form $m_x = m_{\mathbf{Q}}(\cos(\mathbf{Q}_1 \cdot \mathbf{r}) + \cos(\mathbf{Q}_2 \cdot \mathbf{r}))$. As a possible transition from single-Q to double-Q structure in the coexistence phase seems to be suggested by experiment [4], mapping out the phase diagram for this model seems quite relevant.

Going beyond the work done here, a logical next step is to map out the induced magnetization in finite field. We find that a strong impurity in a substantial field induces the transverse magnetization locally. This proof of concept suggests the homogeneous order could be induced by a collection of such impurities and the Q phase thus expanded, a process very relevant to the doping of $CeCoIn_5$ by magnetic impurities.

# 7. Conclusion

In summary, we have shown how the nodal structure of the d-wave ordering gap in $CeCoIn_5$ under magnetic field creates nodal pockets of parallel regions on the Fermi surface. These nested regions are unstable to the formation of antiferromagnetic order, illustrating how superconductivity is required for the formation of this order. Through self-consistent simulation we have reproduced the expected phase diagram for this compound. The coexistence phase in this phase diagram shows the order expected from [4]. Studying the lattice ordering of the self-consistent fields in this homogeneous system, we have found modulations corresponding to the nesting vector $\mathbf{Q}$, including an unexpected though non-interfering $m_z$ component.

Including impurities along and orthogonal to the field we have seen how the local $(x)$ component of the magnetization becomes rotationally invariant in contrast to the homogeneous order. We have mapped out the linear magnetization for impurities at $h = 0$ and found a linear mean field relation between impurity potential and strength of the nesting order. Initializing a field below the Q-phase critical field we have induced the $m_x$ magnetization locally using a $(z)$ impurity, in strong correlation with the homogeneous formation of the Q-phase. Finally, we have described how our study of impurity magnetization suggest the possibility of expanding the homogeneous phase through impurity doping.

# References


[1] P. Coleman. Heavy fermions: electrons at the edge of magnetism Center For Materials Theory, Rutgers University, Piscataway, NJ. arXiv:cond-mat/0612006v3, 2006.

[2] J. W. Harter. Numerical modeling of impurity-induced magnetic behavior in cuprate superconductors Bachelor's thesis, Department of Physics , University of Florida, Gainesville, FL, April 2006.

[3] A. C. Hewson. The Kondo Problem to Heavy Fermions. Cambridge University Press, Cambridge, 2003.

[4] Y. Kato, C. D. Batista, and I. Vekhter. Antiferromagnetic order in pauli-limited unconventional superconductor. Phys. Rev. Lett., 107(096401), 2011.

[5] M. P. Marder. Condensed Matter Physics. Wiley-Interscience, 2000.

[6] Y. Matsuda and H. Shimahara. Fulde–ferrell–larkin–ovchinnikov state in heavy fermion superconductors. J. Phys. Soc. Jpn., 76(051005), 2007.

[7] R. D. Mattuck. A Guide to Feynman Diagrams in the Many-Body Problem (Second Edition). Dover Publications, 1992.



**Acknowledgements**

I would like to express my great appreciation to Brian M. Andersen[1] and Maria N. Gastiasoro[1] for tireless guidance sessions, and for their swift and constructive feedback on far-ranging subjects.
I would also like to thank Ilya Vekhter[2] for his helpful correspondence on the final subject of impurity magnetization.



[1] *Niels Bohr Institute, University of Copenhagen*
[2] *Department of Physics and Astronomy, Louisiana State University*

# A. Calculation of self-consistent fields

The self-consistent fields are calculated using the Bogoliubov transformation. We note the distribution $\langle \gamma^\dagger_{n\sigma}\gamma_{n\sigma}\rangle = f(E_n)$. The anticommutation relations for fermion will allow us to shift operators, allowing terms to be rewritten:

$$\langle \gamma_{n\sigma}\gamma^\dagger_{n\sigma}\rangle = 1 - \langle \gamma^\dagger_{n\sigma}\gamma_{n\sigma}\rangle \tag{A.1}$$
$$= 1 - f(E_n) \tag{A.2}$$
$$= f(-E_n) \tag{A.3}$$

With this in place we now write the self-consistent fields in terms of quasiparticle operators, then use the conjugate transpose to obtain expressions independent of any sorting of eigenvalues and eigenvectors, i.e. we require that the fields can be written as a single sum over $n$. To pair operators with the corresponding energies we first write out the condition that the $\gamma$ operators diagonalize the Hamiltonian:

$$H = \sum_n E_n\gamma^\dagger_{n\uparrow}\gamma_{n\uparrow} + E_{n+N^2}\gamma_{n\downarrow}\gamma^\dagger_{n\downarrow} + E_{n+2N^2}\gamma^\dagger_{n\downarrow}\gamma_{n\downarrow} + E_{n+3N^2}\gamma_{n\uparrow}\gamma^\dagger_{n\uparrow} \tag{A.4}$$

This tells us the energy corresponding to the product of operators, e.g. $\langle \gamma_{n\downarrow}\gamma^\dagger_{n\downarrow}\rangle = f(E_{n+N^2})$.

The density operator demonstrates the general method:

$$n_{i\uparrow} = \langle c^\dagger_{i\uparrow}c_{i\uparrow}\rangle \tag{A.5}$$
$$= \langle (c_{i\uparrow})^\dagger c_{i\uparrow}\rangle \tag{A.6}$$
$$= \langle (\sum_{n=1}^{N^2} \alpha^*_{in}\gamma^\dagger_{n\uparrow} + \alpha^*_{i,N^2+n}\gamma_{n\uparrow} + \alpha^*_{i,2N^2+n}\gamma^\dagger_{n\uparrow} + \alpha^*_{i,3N^2+n}\gamma_{n\uparrow}) \tag{A.7}$$
$$(\sum_{n=1}^{N^2} \alpha_{in}\gamma_{n\uparrow} + \alpha_{i,N^2+n}\gamma^\dagger_{n\uparrow} + \alpha_{i,2N^2+n}\gamma_{n\uparrow} + \alpha_{i,3N^2+n}\gamma^\dagger_{n\uparrow})\rangle \tag{A.8}$$
$$= \sum_n^{N^2} |\alpha^1_{in}|^2 f(E_n) + |\alpha^2_{in}|^2 f(E_{n+N^2}) + |\alpha^3_{in}|^2 f(E_{n+2N^2}) + |\alpha^4_{in}|^2 f(E_{n+3N^2}) \tag{A.9}$$
$$= \sum_{n=1}^{4N^2} |\alpha_{in}|^2 f(E_n) \tag{A.10}$$

The other order parameters are written in the same way, using conjugate transposition to obtain an expression applicable to a single sum over $n$.

# B. Mathematica Script

Mathematica is used for the self-consistent calculations.
The script does the following:

1. Initialize self-consistent fields, set parameters
2. Construct Hamiltonian, diagonalize Hamiltonian
3. Update self-consistent fields
4. Print plots of evolution of specific self-consistent fields every few iterations
5. Iterate and go to 2

```
SetDirectory[NotebookDirectory[]];
i = 0; (*Position lists for real space and k space*)
For[iy = 1, iy ≤ Nx, iy++,
For[ix = 1, ix ≤ Nx, ix++, i++;
xpos[i] = ix;
ypos[i] = iy;]];
yposlist = Table[Nx − i, {i, 0, Nx − 1}];
xposlist = Table[i, {i, 1, Nx}];
kxList = Table[l ∗ Pi/(Nx/2), {l, −Nx/2, Nx/2}];
kyList = kxList;
(*Parameters*)
ChemPot0 = 0.68;
ChemPot = ChemPot0;
ChemLoopMaxIt = 200;
jPot = 3.5 ∗ t;
hPot = 0. ∗ t;
mQ = 0. ∗ t;
Q = 0.8888 ∗ Pi;
vPot = 3. ∗ t;
```

```
vImp = 2. * t;
ImpType = x;
ImpSite = If[Mod[Nx, 2] == 1, Ceiling[0.5 * Nx^2 - Nx/2], Ceiling[0.5 * Nx^2];]
(*Place impurity in the middle of lattice*)
HLength = (4Nx^2);
inSpinFactorA = 1;
inSpinFactorB = 1;
nTotalCalc = 0.;
kT = 0.01;
DataOld = "Map2"; (*Import and export data*)
DataNew = "Map2";
dWaveModifier = 1; (*0 → sWave, 1 → dWave*)
ImportModifier = 1;
If[ImportModifier == 1,
DeltaSC = Get[StringJoin["DeltaSC", DataOld]];
AFMMF = Get[StringJoin["AFMMF", DataOld]];
AFMMF = 0.5 * AFMMF;
nSiteUp = Get[StringJoin["nSiteUp", DataOld]];
nSiteDown = Get[StringJoin["nSiteDown", DataOld]];
nTotalCalc = Get[StringJoin["nTotalCalc", DataOld]];
DeltaSCCalc = Table[0, {i, 1, 4}, {j, 1, Nx^2}];
,
If[dWaveModifier == 1,
DeltaSC = Table[If[i < 3, 0.4, -0.4], {i, 1, 4}, {j, 1, Nx^2}];
DeltaSCCalc = Table[0, {i, 1, 4}, {j, 1, Nx^2}];
,
DeltaSC = Table[1, {i, 1, Nx^2}]; DeltaSCCalc = Table[0, {i, 1, Nx^2}]
];
DeltaSCCalc = Table[0, {i, 1, 4}, {j, 1, Nx^2}];
AFMMF0 = 0.5 * Table[mQ * Cos[((xpos[i]) * Q + (ypos[i]) * Q)], {i, 1, Nx^2}]; (*updagger down*);
AFMMF = AFMMF0;
```

```
nSiteUp = 1/2 * Table[If[EvenQ[xpos[i] + ypos[i]], inSpinFactorB, inSpinFactorA], {i, Nx^2}];
nSiteDown = 1/2 * Table[If[EvenQ[xpos[i] + ypos[i]], inSpinFactorA, inSpinFactorB], {i, Nx^2}];
];
nSiteUpCalc = Table[0, {i, 1, Nx^2}]; nSiteDownCalc = Table[0, {i, 1, Nx^2}];
AFMMFCalc = Table[0, {i, 1, Nx^2}];

AFMList = {Re[AFMMF[[3]] + Conjugate[AFMMF[[3]]]]}; (*Define inspection lists*)
DeltaSCList = {Re[DeltaSC[[1, 1]]]};
AFMListImp = {Re[AFMMF[[ImpSite]] + Conjugate[AFMMF[[ImpSite]]]]};
mSiteList = {(nSiteUpCalc[[ImpSite]] - nSiteDownCalc[[ImpSite]])};
(*definenearestneighboursunderperiodicboundaryconditions, leftrightupdown*)
NearNeigh[i_]:={
Switch[Mod[i - 1, Nx], 0, i - 1 + Nx, _, i - 1],
Switch[Mod[i, Nx], 0, i + 1 - Nx, _, i + 1],
Switch[Sign[Nx + 1 - i], 1, Nx^2 - (Nx - i), _, i - Nx],
Switch[Sign[i - (Nx - 1) * Nx], 1, i - (Nx - 1) * Nx, _, i + Nx]
};
i = 1;
FermiDistLimit[E_]:=1/(Exp[E/kT] + 1);

Print[TableForm[{{J, h, "kT"}, {jPot, hPot, kT}}]];
a = 1;
Print[{" ChemPot ", "nTotalCalc"}]
While[a < ChemLoopMaxIt + 1,

H = Table[0, {l, 1, HLength}, {j, 1, HLength}];

j = 1; i = 1;
While[j < Nx^2 + 1,
H[[i, j]] = -ChemPot - hPot;
H[[i + Nx^2, j + Nx^2]] = ChemPot - hPot;
```

```
H[[i + 2Nx^2, j + 2Nx^2]] = -ChemPot + hPot;
H[[i + 3Nx^2, j + 3Nx^2]] = ChemPot + hPot;

H[[i, NearNeigh[j]]] = -t;
H[[i + Nx^2, Nx^2 + NearNeigh[j]]] = t;
H[[i + 2Nx^2, 2Nx^2 + NearNeigh[j]]] = -t;
H[[i + 3Nx^2, 3Nx^2 + NearNeigh[j]]] = t;

H[[i, j + 2Nx^2]] = -jPot * AFMMF[[j]];
H[[i + Nx^2, j + 3Nx^2]] = jPot * AFMMF[[j]];
H[[i + 2Nx^2, j]] = -jPot * Conjugate[AFMMF[[j]]];
H[[i + 3Nx^2, j + Nx^2]] = jPot * Conjugate[AFMMF[[j]]];

H[[NearNeigh[j], j + Nx^2]] = Conjugate[{DeltaSC[[1, j]], DeltaSC[[2, j]], DeltaSC[[3, j]], DeltaSC[[4, j]]}];
H[[i + Nx^2, NearNeigh[j]]] = {DeltaSC[[1, j]], DeltaSC[[2, j]], DeltaSC[[3, j]], DeltaSC[[4, j]]};
H[[NearNeigh[i] + 2Nx^2, 3Nx^2 + j ]] = -Conjugate[{DeltaSC[[1, j]], DeltaSC[[2, j]], DeltaSC[[3, j]], DeltaSC[[4, j]]}
H[[i + 3Nx^2, NearNeigh[j] + 2Nx^2]] = -{DeltaSC[[1, j]], DeltaSC[[2, j]], DeltaSC[[3, j]], DeltaSC[[4, j]]};

i++; j++];
If[ImpType == x,
H[[ImpSite, ImpSite + 2Nx^2]] = H[[ImpSite, ImpSite + 2Nx^2]] - vImp;
H[[ImpSite + Nx^2, ImpSite + 3Nx^2]] = H[[ImpSite + Nx^2, ImpSite + 3Nx^2]] + vImp;
H[[ImpSite + 2Nx^2, ImpSite]] = H[[ImpSite + 2Nx^2, ImpSite]] - vImp;
H[[ImpSite + 3Nx^2, ImpSite + Nx^2]] = H[[ImpSite + 3Nx^2, ImpSite + Nx^2]] + vImp;
,
H[[ImpSite, ImpSite]] = H[[ImpSite, ImpSite]] - vImp;
H[[ImpSite + Nx^2, ImpSite + Nx^2]] = H[[ImpSite + Nx^2, ImpSite + Nx^2]] - vImp;
H[[ImpSite + 2Nx^2, ImpSite + 2Nx^2]] = H[[ImpSite + 2Nx^2, ImpSite + 2Nx^2]] + vImp;
H[[ImpSite + 3Nx^2, ImpSite + 3Nx^2]] = H[[ImpSite + 3Nx^2, ImpSite + 3Nx^2]] + vImp; ];

H = Chop[H]; EigH = Eigensystem[H];
```

```
U = Transpose[EigH[[2, 1;;4Nx^2, 1;;4Nx^2]]];

alpha = U[[1;;Nx^2, 1;;HLength]];
beta = U[[Nx^2 + 1;;2 * Nx^2, 1;;HLength]];
omega = U[[2 * Nx^2 + 1;;3 * Nx^2, 1;;HLength]];
uvar = U[[3 * Nx^2 + 1;;4 * Nx^2, 1;;HLength]];



nSiteUpCalc = Table[Total[
Table[
Abs[alpha[[i, n]]]^2 * FermiDistLimit[EigH[[1, n]]]
, {n, 1, 4Nx^2}]], {i, 1, Nx^2}];

nSiteDownCalc = Table[Total[
Table[
Abs[omega[[i, n]]]^2 * FermiDistLimit[EigH[[1, n]]]
, {n, 1, 4Nx^2}]
], {i, 1, Nx^2}];

AFMMFCalc = Table[Total[
Table[
uvar[[i, n]] * Conjugate[beta[[i, n]]] * FermiDistLimit[-EigH[[1, n]]]
, {n, 1, 4Nx^2}]
], {i, 1, Nx^2}];

If[dWaveModifier == 1,
l = 1;
While[l < 5,
DeltaSCCalc[[l]] = Table[vPot * Total[
Table[
alpha[[i, n]] * Conjugate[beta[[NearNeigh[i][[l]], n]]] * FermiDistLimit[-EigH[[1, n]]]
```

```
, {n, 1, 4Nx^2}]
], {i, 1, Nx^2}];
l++],
DeltaSCCalc = Table[vPot * Total[
Table[alpha[[i, n]] * Conjugate[beta[[i, n]]] * FermiDistLimit[-EigH[[1, n]]]
, {n, 1, 4Nx^2}]
], {i, 1, Nx^2}];
];
nSiteCalc = Table[nSiteUpCalc[[i]] + nSiteDownCalc[[i]], {i, 1, Nx^2}];
nTotalCalc = (1/(Nx^2))(Total[nSiteUpCalc] + Total[nSiteDownCalc]);

AppendTo[AFMListImp, Re[(AFMMF[[ImpSite]] + Conjugate[AFMMF[[ImpSite]]])]];
AppendTo[AFMList, Re[(AFMMF[[3]] + Conjugate[AFMMF[[3]]])]];
AppendTo[DeltaSCList, Re[DeltaSC[[1, 1]]]];
AppendTo[mSiteList, (nSiteUpCalc[[ImpSite]] - nSiteDownCalc[[ImpSite]])];

(*Print inspection lists and initial plots of the order*)
If[Mod[a, 10] - 1 == 1,
ff = Table[Total[Table[(nSiteUpCalc[[i]] - nSiteDownCalc[[i]]) * Exp[I((kx * (xpos[i]) + ky * (ypos[i])))],
{i, 1, Nx^2}]], {kx, kxList}, {ky, kyList}]/(Nx^2);
bb = Sqrt[Abs[Re[ff]]^2 + Abs[Im[ff]]^2];
Print[ListDensityPlot[bb, ColorFunction → "Temperature",
PlotLegends → Automatic, PlotRange → All, Mesh → False, Frame → {True, True, None, None},
FrameTicks → {{{1, "-π"}, {10, "kx"}, {19, "π"}}, {{1, "-π"}, {10, "ky"}, {19, "π"}}, None, None},
FrameStyle → Directive[16]]];
Print[ListPlot[mSiteList, PlotRange → {0, 1.3}, PlotLabel → {Mz}]];
Print[ListPlot[{AFMList, Abs[AFMListImp]}, PlotRange → {0, 0.7},
PlotStyle → {PointSize[Small], PointSize[Medium]}]];
Print[ListPlot[DeltaSCList, PlotRange → {0, 0.7}]];
Print[ArrayPlot[Table[nSiteUpCalc[[(y - 1) * Nx + x]] - nSiteDownCalc[[(y - 1) * Nx + x]]
, {y, yposlist}, {x, xposlist}], ColorFunction → "Temperature", PlotLegends → Automatic]];
```

```
nSiteUp = 0.4 * nSiteUp + 0.6 * nSiteUpCalc;
nSiteDown = 0.4 * nSiteDown + 0.6 * nSiteDownCalc;
AFMMF = 0.4AFMMF + 0.6AFMMFCalc;
DeltaSC = 0.4 * DeltaSC + 0.6 * DeltaSCCalc;

If[Mod[a, 10] == 1,
PamSet = {hPot, vImp, kT};
Save[StringJoin["nSiteUp", DataNew], nSiteUp];
Save[StringJoin["nSiteDown", DataNew], nSiteDown];
Save[StringJoin["DeltaSC", DataNew], DeltaSC];
Save[StringJoin["AFMMF", DataNew], AFMMF];
Save[StringJoin["nTotalCalc", DataNew], nTotalCalc];
Save[StringJoin["PamSet", DataNew], PamSet]; ];

a++];
```

# C. Magnetization Vector Plot